Mean-Squared Error Beamforming for Coherent Plane-Wave Compounding

Nghia Q. Nguyen
Department of Engineering
University of Cambridge
Cambridge, United Kingdom
nqn20@cam.ac.uk

Richard W. Prager
Department of Engineering
University of Cambridge
Cambridge, United Kingdom
rwp@eng.cam.ac.uk

***Abstract*—The goal of this paper is to implement a new *minimum mean-squared error* (MMSE) beamformer for coherent plane-wave compounding. In ultrasound imaging, an beamformer, in the MMSE approach, is usually derived as a multiplication of the *minimum variance distortionless response* (MVDR) output and a scalar, which is approximated by the *coherent factor* (CF). Beside the spatial smoothing adopted for estimating the data covariance matrix in MVDR beamforming, this approximation could be another factor that potentially reduces performance of the MMSE. In this paper, we extend the spatial coherent approach that we developed previously for MVDR beamforming, and show how this scalar can be estimated through an array of MVDR outputs. Advances of the proposed MMSE are evaluated on datasets available on PICMUS website. The imaging results show it offers improvements, in terms of spatial and contrast resolution, over the corresponding MVDR and a combination of MVDR beamforming and CF in the literature.**

***Index Terms*—ultrasound, beamforming, minimum variance, minimum mean-squared error, image quality**

I. Introduction

Advances in data storage and computational technology make it realistic to consider implementing "gold standard" beamformers for ultrasound imaging systems, i.e., the pulse-echo beam is generated with focussing on both transmit and receive over the entire imaging region [1]. One of such imaging systems is the coherent plane-wave compounding (CPWC). While the receive focusing is still achieved through the dynamic time-delay calculations, the transmit focusing is synthesized by steering the plane-wave beam in different directions, where backscattered signals are compounded coherently. Currently, the data superposition is stilled processed through a simple *delay-and-sum* (DAS) algorithm [2]. It is fast and robust but compromises image quality.

Attempts to improve the ultrasound image resolution usually lead to the use of *minimum variance distortionless response* (MVDR) and *minimum-mean-squared-error* (MMSE) beamforming. The former approach involves coefficients that weight the echo signals before adding them together. Calculating those weights requires an inversion of the data covariance matrix. It has a problem because the estimation of this matrix is based on only one vector sample of the data, or *snapshot*, available. Beamformer performance, therefore, is limited by a lack of robustness to estimated errors. There are several techniques to overcome this issue. The most popular approach is the *spatial smoothing* approximation which divides the data vector into smaller overlapping subarrays so that several snapshots can be created [3]. To avoid ill-conditioning, the number of snapshots should be greater than or equal to the matrix size. This limits the subarray length to less than or equal to half of the vector length. Spatial smoothing has been shown to enhance beamformer robustness. However, it increases the computational load and reduces the effective aperture which affects image resolutions. In the latter approach of using MMSE criterion, the beamformer is usually factorized into a MVDR beamformer output and a scalar. In most related studies, the scalar is approximated to a coherence factor (CF) or its modifications calculated based on the received data vector. It was showed that the CF helps improve the imaging contrast but creating some undesired artefacts surround the hyperechoic regions of the images [4].

Previously, we have developed the MVDR for the CPWC systems [5]. The unique of our approach is to consider the MVDR beamformer as a deconvolution filter that decorrelates the correlation among echo signals received on individual elements. We have found a new method to estimate the data covariance matrix by approximating the correlations of signals to the spatial coherence among them. Through the PICMUS datasets [6], we showed the MVDR beamformer, implemented with this new estimation, outperforms the DAS beamformer and other existing MVDR-based algorithms. In this paper, we develop a new MMSE beamformer by extending this work. We are motivated by a finding in our information-theoretic framework that the Wiener-filtered or MMSE beamformer outperforms the MVDR especially under low eSNR conditions of imaging data. We compare the new method to the DAS, the corresponding MVDR, and another similar strategy drawn from the literature. Beamformers are assessed through the quality of imaging results generated based on PICMUS datasets [6]. From this perspective, strengths of our new MMSE beamformer will be evaluated and analyzed.

II. Methods

A. Coherent Plane-wave Compounding

In CPWC, data are acquired by insonifying with plane-wave beams in multiple directions over the entire imaging

region [2]. By assuming the transmit beam is steered in M different angles and backscattered waveforms are received on an N-element linear array, the signals with time index n, after appropriate delays for the specific pixel under consideration, can be arranged in a 2-D matrix $\mathbf{X}(n)$ of $M \times N$, given by

$$\mathbf{X}(n) = \begin{bmatrix} x_{1,1}(n) & x_{1,2}(n) & \cdots & x_{1,N}(n) \\ x_{2,1}(n) & x_{2,2}(n) & \cdots & x_{2,N}(n) \\ \vdots & \vdots & \ddots & \vdots \\ x_{M,1}(n) & x_{M,2} & \cdots & x_{M,N}(n) \end{bmatrix}, \quad (1)$$

where $x_{ij}(n)$ is the signal received on channel j after a transmitted excitation at firing angle i. The compounded data or DAS beamformer output is given as

$$y_{\mathrm{CPWC}}(n) = \frac{1}{MN} \sum_{i=1}^{M} \sum_{j=1}^{N} x_{ij}(n) \ . \quad (2)$$

B. Minimum Variance Beamforming and Coherent Factor

We follow the study in [4] to form a MMSE strategy by combining a MVDR beamformer with a coherent factor. The first MVDR beamformer applied to CPWC is used to combine low-resolution images each generated by a DAS beamformer within one plane-wave transmit [9]. By arranging the collected data into matrix $\mathbf{X}(n)$, this strategy is equivalent to applying MVDR to a vector that is composed of sums over individual rows of the matrix. We denote this vector as $\mathbf{u}(n) = [u_1(n), u_2(n), ..., u_M(n)]^T$, where $u_i(n)$ is given by

$$u_i(n) = \sum_{j=1}^{N} x_{i,j}(n) \quad \text{for } i = \overline{1, M} \ . \quad (3)$$

The MVDR applied to $\mathbf{u}(n)$ is implemented through the spatial smoothing approach with the details provided in [9]. We combine the output of this beamformer to the CF, calculated as a ratio of the coherent sum over the incoherent sum of $\mathbf{u}(n)$, given by

$$\mathrm{CF}(n) = \frac{\left| \sum_{i=1}^{M} u_i(n) \right|^2}{M \sum_{i=1}^{M} |u_i(n)|^2} \ . \quad (4)$$

In this paper, we denote this strategy as an *MVDR+CF* beamformer.

C. Data-Compounded-among-Transmit MVDR [5]

In [5], we develop a new MVDR applied to data after compounded over multiple transmits. Alternatively, it is equivalent to a data vector after superposition among all rows of $\mathbf{X}(n)$. We denote it by $\mathbf{v}(n) = [v_1(n), v_2(n), ..., v_N(n)]^T$ where

$$v_j(n) = \sum_{i=1}^{M} x_{i,j}(n) \quad \text{for } j = \overline{1, N} \ , \quad (5)$$

which is the summed signals on element j over all transmit events.

The unique of our MVDR implementation is that we estimate the covariance matrix of $\mathbf{v}(n)$ through a new set of snapshot $\mathbf{p}_k(n) = [p_{k,1}(n), p_{k,2}(n), ..., p_{k,N}(n)]^T$, where

$$p_{k,j}(n) = \frac{1}{M-1} \sum_{\substack{i=1 \\ i \neq k}}^{M} x_{i,j}(n) \ . \quad (6)$$

Vector $\mathbf{p}_k(n)$ is still composed of compounded data like $\mathbf{v}(n)$ but excluding echo signals from transmit event k. The statistical similarity between $\mathbf{v}(n)$ and $\mathbf{p}_k(n)$ can be described details in [5]. An advantage of this estimation is that the snapshots still have the same size to that of the input vector. Thus, the aperture size is still preserved through the MVDR implementation. As the snapshots are generated by using data compounded among multiple transmits, we name it *data-compounded-among-transmit MVDR* (DCT-MVDR).

D. Data-Compounded-among-Transmit MMSE

We form a new MMSE beamformer by multiplying the DCT-MVDR output to a scalar. We calculate that scalar in the way similar to Eq. (4), but through an array of MVDR outputs instead of the receive data vector. We first denote $\mathbf{w}_{\mathrm{DCT}}$ as the weight vector of the DCT-MVDR, from the snapshots $\mathbf{p}_k(n)$, we form an array of $q_k(n)$ as

$$q_k(n) = \mathbf{w}_{\mathrm{DCT}}^t \, \mathbf{p}_k(n) \ . \quad (7)$$

The new factor is calculated by,

$$\mathrm{CF}_{\mathrm{MVDR}}(n) = \frac{\left| \sum_{k=1}^{M} q_k(n) \right|^2}{M \sum_{k=1}^{M} |q_k(n)|^2} \ . \quad (8)$$

Combining this $\mathrm{CF}_{\mathrm{MVDR}}(n)$ to the DCT-MVDR output, we able to form a new MMSE beamformer applied to the CPWC. We name it *data-compounded-among-transmit MMSE* (DCT-MMSE) beamformer.

III. Results

A. Data Acquisition and Evaluation Metrics

We demonstrate the beamformers on imaging data provided by the Plane-wave Imaging Challenge in Medical Ultrasound (PICMUS) [6]. The datasets were recorded using a Verasonics Vantage 256 research scanner and L11 probe (Verasonics Inc., Redmond, WA). It also includes simulations of point-targets with Field II [10] configured to model the same system. Details of the system configuration are provided in [6].

We evaluate each beamformer based on the spatial and contrast resolution of the generated images. The spatial resolution is quantified using the responses of each beamformer to individual scatterers. Because all MVDR-based beamformers are developed based on an assumption of narrow-band signals that ignores temporal correlation, they mainly improve the lateral resolution. Thus, we are interested in the full width at half maximum (FWHM) of the response in the lateral direction

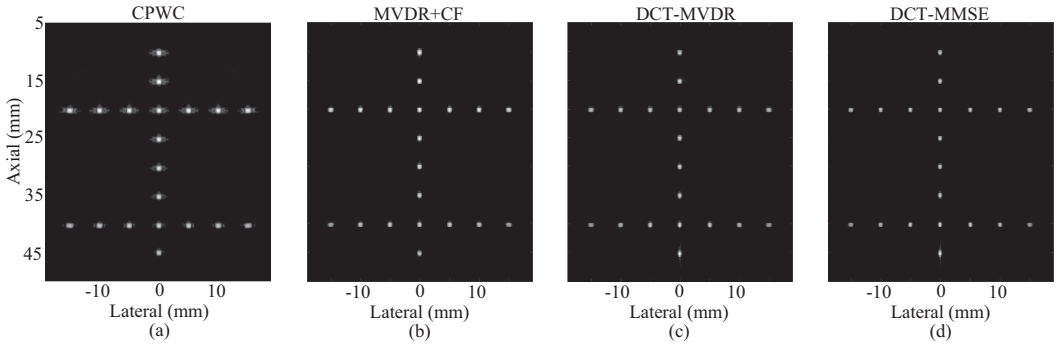

Fig. 1. Simulated images of 9 idealized lesions generated with different beamformers: (a) CPWC, (b) MVDR+CF, (c) DCT-MVDR, and (d) DCT-MMSE. All images are log-compressed and displayed with a dynamic range of 60 dB.

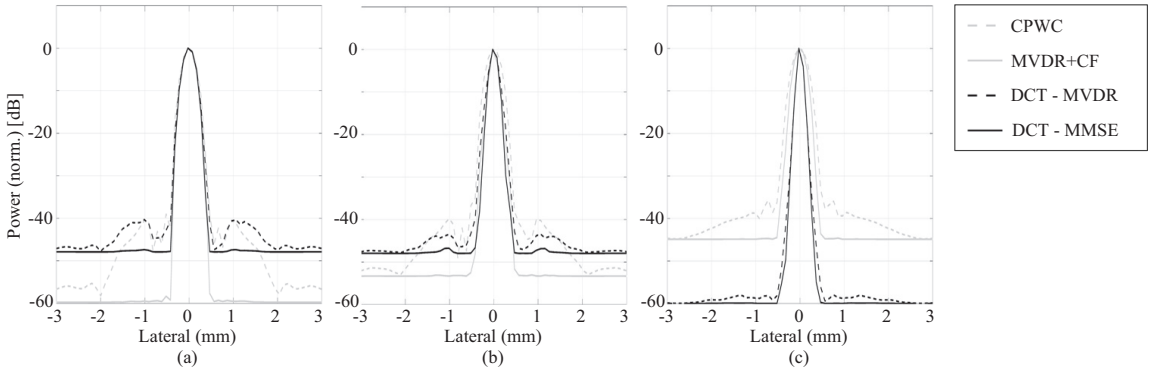

Fig. 2. Lateral responses to point-targets at different depths: (a) 15 mm, (b) 30 mm, and (c) 45 mm. The beamformers are: CPWC, MVDR+CF, DCT-MVDR, and DCT-MMSE. The legend at the right side applies to all plots.

only. The contrast resolution is measured using the contrast ratio (CR) between a lesion and the background, given by

$$\mathrm{CR} = \frac{I_{out} - I_{in}}{\sqrt{I_{out}^2 + I_{in}^2}}\,, \tag{9}$$

where I_{in} and I_{out} are the mean intensities (in decibels) measured inside and outside the lesion, respectively. The term CR has a value of 1 for perfect contrast, and a value of 0 for no contrast between the lesion and background. The background kernel is selected as a circular ring enclosing the lesion with an area that is the same as that of the lesion. This helps to minimise the effects of variations in the attenuation and diffraction of the ultrasound.

B. Simulated Point-Targets

We evaluate the beamformer performance on simulated data generated with 20 point-targets. Eight of them are located in the center of the image, ranged from 10 mm to 45 mm with a 5 mm separation. There are also two sets of 7 point-targets at depths of 20 mm and 40 mm. In each of these sets, the points are evenly distributed from -15 mm to 15 mm in the lateral direction.

Figures 1(a)–(d) show the images generated with the CPWC, MVDR+CF, DCT-MVDR, and DCT-MMSE beamformers, respectively. In the figures, the CPWC image has the most blurring point-targets. The DCT-MVDR has poor resolutions in the near-field region as consistently showed in our previous study [5]. In all plots, the DCT-MMSE helps reduce the sidelobes while having its mainlobes maintained or even slightly better than those obtained with the DCT-MVDR. We quantify the image quality using the FWHMs measured through the mainlobes of the beamformer responses in Figs. 1. The averaged results are summarized in Table I.

To show the performance of the beamformers in more details, we plot their lateral responses to some of the point-targets in Figs. 2(a)–(c). These are the responses to the central points at depths of 15 mm, 30 mm, and 45 mm, respectively. The plots show that all the MVDR-based algorithms, help reduce the mainlobes and suppress the sidelobes compared to CPWC.

C. Phantom Study

We apply the beamformers to experimental data acquired by scanning a multi-purpose tissue-mimicking phantom (model 040GSE, CIRS, Norfolk, VA, USA) [6]. The manufacturer reported a sound speed of 1540 $\pm$ 10 m/s and a background attenuation coefficient slope of $0.5\,\mathrm{dB\,cm^{-1}MHz^{-1}}$. This dataset is designed to assess the performance on contrast resolution of each beamformer. The scanned imaging data includes two anechoic cysts against a speckle background. The

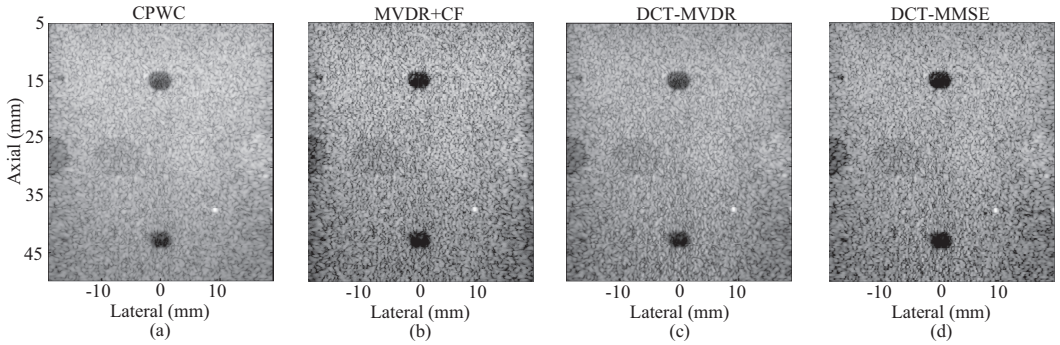

Fig. 3. Experimental images for contrast evaluation generated with the different beamformers: (a) CPWC, (b) MVDR+CF, (c) DCT-MVDR, and (d) DCT-MMSE. All images are log-compressed and displayed with a dynamic range of 70 dB.

TABLE I
PERFORMANCE METRICS MEASURED ON BEAMFORMED IMAGES FROM SIMULTATION, PHANTOM AND IN VIVO STUDIES

Beamformer	average FWHM	near-field CR	far-field CR
CPWC	0.44 $\pm$ 0.06 mm	0.470	0.547
MVDR+CF	0.34 $\pm$ 0.22 mm	0.825	0.779
DCT-MVDR	0.33 $\pm$ 0.17 mm	0.567	0.683
DCT-MMSE	0.30 $\pm$ 0.15 mm	0.886	0.829

cysts are 3 mm in diameter, positioned at depths around 15 mm and 45 mm. Images generated with the beamforming strategies are shown in Figs. 3(a)-(d). In these figures, the contrast ratios of CPWC and DCT-MVDR are low. Combining to the CF helps the CPWC enhance contrast resolution significantly. The best contrast resolution, however, is with the DCT-MMSE. The resolution is improved significantly compared to the DCT-MVDR especially in the near-field region. We measure the CRs on each cysts (near-field CR and far-field CR) and summarize the results in Table I.

IV. CONCLUSION

The findings on imaging results are consistent with those discovered in our information-theoretic framework [7], [8]. In that task-based framework, we have found the MMSE outperforms the MVDR especially on the contrast-related task and under low echo SNR of data. In this study, the better performance of the MMSE is illustrated through the suppression of the sidelobes on the point-target responses and the significant improvements of lesion contrasts, especially in the near-field region. It could be explained that our methods are developed based on an assumption of an spherical wave for each of the plane-wave transmissions. In the near-field, there are some artefacts that affect to the validity of that assumption. They could be recast as noise imposing on imaging data. As a result, the MVDR has a poor performance in the near-field. In that case, the MMSE can help improve the imaging contrast significantly. In far-field region where the MVDR has higher performance, the MMSE still help enhance the image resolutions, but the improvements are reduced compared to the near-field region.

In the next step, we are going to apply the new MMSE to *in vivo* data to verify its robustness toward the phase aberrations. In this paper, the MMSE is applied to a data set with 75 plane-wave transmissions. The large number of steering angles could affect the frame-rate of the system and reduce its potential in some applications of ultrasound imaging. We are keen on applying this technique with a smaller number of plane-wave transmissions. That helps overcome the trade-offs between temporal resolution and image quality in coherent plane-wave imaging.

REFERENCES

[1] K. E. Thomenius, "Evolution of ultrasound beamformers," *Proceedings of the IEEE Ultrasonics Symposium*., pp. 1615-1622, 1996.
[2] G. Montaldo, M. Tanter, J. Bercoff, N. Benech, and M. Fink, "Coherent plane-wave compounding for very high frame rate ultrasonography and transient elastography" in *IEEE Trans Ultrason Ferroelec Freq Control*, vol. 56, no. 3, pp. 489-506, 2009.
[3] J.-F. Synnevåg, A. Austeng, and S. Holm, "Adaptive beamforming applied to medical ultrasound imaging," *IEEE Transactions on Ultrasonics, Ferroelectrics, and Frequency Control*, vol. 54, no. 8, pp. 1606–1613, 2007.
[4] C.-I.C. Nilsen and S. Holm, "Wiener beamforming and the coherence factor in ultrasound imaging," *IEEE Transactions on Ultrasonics, Ferroelectrics, and Frequency Control*, vol. 57, no. 6, pp. 1329–1346, 2010.
[5] N.Q. Nguyen and R.W. Prager, "A spatial coherence approach to minimum variance beamforming for plane-wave compounding," *IEEE Transactions on Ultrasonics, Ferroelectrics, and Frequency Control*, vol. 65, no. 4, pp. 522–534, 2018.
[6] H. Liebgott, A. Rodriguez-Molares, F. Cervenansky, J.A. Jensen, and O. Bernard, "Plane-wave imaging challenge in medical ultrasound," in *Proceedings of the IEEE Ultrasonics Symposium*, pp. 1–4, 2016.
[7] N.Q. Nguyen, R.W. Prager, and M.F. Insana, "A task-based analytical framework for ultrasonic beamformer comparison," in *Journal of the Acoustical Society of America*, vol. 140, no. 2, pp. 1048-1059, 2016.
[8] N.Q. Nguyen, R.W. Prager, and M.F. Insana, "Improvements to ultrasonic beamformer design and implementation derived from the task-based analytical framework," in *Journal of the Acoustical Society of America*, vol. 141, no. 6, pp. 4427-4437, 2017.
[9] A. Austeng, C.-I.C. Nilsen, A.C. Jensen, S.P. Näsholm, and S. Holm, "Coherent plane-wave compounding and minimum variance beamforming," in *Proceedings of the IEEE Ultrasonics Symposium*, pp. 2448–2451, 2011.
[10] J.A. Jensen and N.B. Svendsen, "Calculation of pressure fields from arbitrarily shaped, apodized, and excited ultrasound transducers," *IEEE Trans Ultrason Ferroelec Freq Control*, vol. 39, no. 2, pp. 262–267, 1992.